行政院國家科學委員會專題研究計畫 成果報告

以微機電技術建構之自由空間光通訊系統—用於無人飛行載具或人造衛星間之訊息傳輸
研究成果報告(精簡版)

計 畫 類 別 ：個別型
計 畫 編 號 ：NSC 95-2221-E-002-053-
執 行 期 間 ：95 年 08 月 01 日至 96 年 10 月 31 日
執 行 單 位 ：國立臺灣大學光電工程學研究所

計 畫 主 持 人：蔡睿哲

計畫參與人員：博士班研究生-兼任助理：廖均達
碩士班研究生-兼任助理：余宗翰、謝典良、吳峻名、呂理誠、尹淳義、賴仁傑、邱聖傑、陳國田

報 告 附 件 ：國外研究心得報告

處 理 方 式 ：本計畫可公開查詢

中 華 民 國 97 年 01 月 31 日

行政院國家科學委員會補助專題研究計畫 ☑ 成 果 報 告
□期中進度報告

以微機電技術建構之自由空間光通訊系統—用於無人飛行載具或人造衛星間之訊息傳輸

計畫類別：☑ 個別型計畫　□ 整合型計畫
計畫編號：NSC 95－2221－E－002－053－
執行期間：　95 年　8 月　1 日至　96 年 10 月 31 日

計畫主持人：蔡睿哲
共同主持人：
計畫參與人員：余宗翰、謝典良、吳峻名、呂理誠、尹淳義、廖均達、賴仁傑、邱聖傑、陳國田〔研究生兼任助理〕

成果報告類型(依經費核定清單規定繳交)：☑精簡報告　□完整報告

本成果報告包括以下應繳交之附件：
☑赴國外出差或研習心得報告一份
□赴大陸地區出差或研習心得報告一份
□出席國際學術會議心得報告及發表之論文各一份
□國際合作研究計畫國外研究報告書一份

處理方式：除產學合作研究計畫、提升產業技術及人才培育研究計畫、列管計畫及下列情形者外，得立即公開查詢
□涉及專利或其他智慧財產權，□一年□二年後可公開查詢

執行單位：國立台灣大學　光電工程學研究所

中　華　民　國　97 年　1 月　30 日

Abstract

A theoretical model based on Fourier optics and the power-coupling overlap integral is built to investigate the inter-channel response in a MEMS (Micro-Electro-Mechanical Systems) $1xN^2$ wavelength-selective switch (WSS). The simulation results demonstrate that the inter-channel response depends significantly on the output port location and the radius of curvature of the micromirrors. For the output originally aligned with the input along the dispersion direction, inter-channel-response suppression can be achieved by rotating the two-dimensional (2D) collimator array by a slight angle, e.g. 20°. Experimental results under different conditions are also shown.

This Fourier-optics-based model can also be used to calculate the far-field optical pattern in a free-space optical communication system.

Key Words—Fourier optics, MEMS mirrors, inter-channel response, free-space optical communication

摘要

我們開發了一個以傅氏光學〔Fourier Optics〕為理論基礎的模型，以分析 $1xN^2$ 波長選擇切換器的通道間響應〔Inter-Channel Response〕。此通道間響應是 WDM 系統中所不希望見到的，而此模型則證實了該響應與輸出埠位置之間的關聯性，因此我們可藉由調整輸出埠的位置來予以抑制。將二維輸入/輸出埠陣列旋轉 20 度，原本位於水平位置的輸出埠其通道間響應之壓抑可達 32.5 dB;此外，通道間響應亦與微鏡片的曲率半徑有關。我們並同時進行實驗以驗證理論模型之正確性。

此以傅氏光學為基礎之理論模型，亦可應用於自由空間光通訊中之遠場光場分布的計算。

關鍵詞—傅氏光學、微鏡片、通道間響應、自由空間光通訊

I. INTRODUCTION (前言)

Dynamic wavelength-selective switches (WSS) have been of great interest as they integrate wavelength demultiplexing, switching, and re-multiplexing functions in compact packages [1-12]. They also enable management of optical networks at the wavelength level and are the building blocks of wavelength-selective crossconnets (WSXC) [1]. A wavelength-selective switch can be realized by various distinct techniques, such as the free-space MEMS (micro-electro-mechanical systems) optical system with a tilting-micromirror array [1-8], the hybrid PLC (planar lightwave circuit)-MEMS architecture [9-11], and liquid crystal-based modules [12].

The ancestor of nowaday free-space MEMS wavelength-selective switches is the MEMS dynamic add-drop multiplexer reported by J. Ford et al [13]. It is essentially a 1x2 wavelength-selective switch. Until now, the maximum output port count for a free-space MEMS 1xN WSS with a one-dimensional (1D) collimator array is N = 4 [1-3]. The port count can be increased from N to N^2 by using a two-dimensional (2D) collimator array in conjunction with a two-axis beam-steering mechanism [4-8]. The two-axis beam steering is implemented by either two linear arrays of one-axis analog micromirrors with orthogonal scanning directions [4], or a monolithic two-axis MEMS scanner array [5-8].

The hybrid PLC-MEMS approach was used by Metconnex (sold to JDS Uniphase Corp. in 2006) to commercially implement a 1x9 WSS [10, 11]. Two PLC chips, each with five input/output ports, were stacked vertically. This architecture is analogous to the free-space MEMS 1xN^2 WSS and also requires a two-axis micromirror array. The same company also offered 1x14 and 1x24 modules [11]. Liquid crystal-based WSS, manufactured by CoAdna Photonics, Inc., is available with a nominal output port count of 8. It can be extended to 1x9, 1x10, or more ports [12].

In our previous study of free-space MEMS 1xN^2 WSS, we observed a large inter-channel response at a horizontal output port which is aligned with the input along the dispersion direction [4]. Similar phenomena have also been discovered in MEMS-based channelized dynamic spectral equalizers with the micromirrors tilting in the dispersion direction [14, 15]. The inter-channel response is undoubtedly undesirable for optical communication. It is preferable to suppress the inter-channel response, therefore maximizing the pass and stop bandwidths, allowing for channel misalignment due to laser drift from the ITU grid, and relaxing packaging requirements. In this paper, we present a theoretical model based upon Fourier optics and the power-coupling overlap integral. The inter-channel response in a MEMS 1xN^2 WSS is investigated and it, according to the simulation results, depends significantly on the output port location and the radius of curvature of the micromirrors. A simple solution is then proposed to suppress the inter-channel response in a 1xN^2 WSS. It can be achieved by rotating the 2D collimator array such that no output port is aligned with the input along the dispersion direction [5]. With 20° rotation, 10-dB and 8.2-dB suppressions are demonstrated theoretically and experimentally, respectively, for a prototype system.

II. THEORETICAL MODEL

Figure 1 shows the schematic of the 1xN^2 WSS. The 2D collimator array is mounted on a

rotary stage with rotation axis parallel to the optical beams. The center collimator serves as the input port. The WDM signals are spatially dispersed by the grating, and focused onto their corresponding mirrors by the resolution lens. The two-axis mirrors direct individual wavelengths to the desired output ports. The telescope beam expander reduces the optical spot size on the MEMS mirror.

The simulation model can be explained with the assistance of Figure 2. For simplicity, the telescope beam expander and the grating are neglected. The field distribution Einput emerging from the input fiber collimator contains both amplitude and phase information. It is projected by the resolution lens to the back focal plane, where the MEMS mirror array is situated. The projected field, denoted by einput, is then spatially modulated by the micromirrors, resulting in a modulated field distribution einput' at the back focal plane. einput' yields a projected field Einput' at the front focal plane, where the collimators are located. The power-coupling efficiency into a specific output fiber collimator is then $\eta = \left| \iint E_{input}' \cdot E^{*}_{output} dxdy \right|^2$, where E_{output} is the modal field distribution of the output collimator [16]. Note that all the field distributions mentioned above are with normalized power, and E_{output} is identical to E_{input} except for a shift in space if all the collimators are identical. Based on Fourier optics [17], E_{input}' and E_{output} are the Fourier transforms of e_{input}' and e_{output}, respectively, where e_{output} is the projected field of the output collimator onto the MEMS device plane (i.e. the back focal plane). According to the properties of the Fourier transform, $\left| \iint E_{input}' \cdot E^{*}_{output} dxdy \right|^2 = \left| \iint e_{input}' \cdot e^{*}_{output} dxdy \right|^2$. Therefore, the power-coupling efficiency can be obtained by calculating the overlap integral $\left| \iint e_{input}' \cdot e^{*}_{output} dxdy \right|^2$, which normally has a much simpler form.

The normalized field distribution e_{output}, the projected image of the output collimator on the MEMS device plane, has a Gaussian shape and is given by

$$e_{output}(x,y,f) = \left(\frac{2}{\pi \omega_{0x} \omega_{0y}} \right)^{1/2} \exp\left[-\frac{\left(x - \frac{pf}{f_0} \right)^2}{\omega_{0x}^{\ 2}} - \frac{y^2}{\omega_{0y}^{\ 2}} \right] \exp\left[jkx \sin\theta_x + jky \sin\theta_y \right] . \quad (1)$$

The parameters used for our simulation are the same as those in the experiment. ω_{0x} and ω_{0y} are the Gaussian beam radii in the x and y directions, respectively. The beam radius emerging from the collimator array is originally 125 μm. It is then expanded to 2 mm after passing through the telescope. This leads to a focused spot on the device plane with ω_{0x} and ω_{0y} being 69 μm and 76 μm, respectively. ω_{0x} and ω_{0y} have different quantities due to the anamorphic effect caused by the diffraction grating. The MEMS mirror pitch (i.e. center-to-center distance between adjacent mirrors), p, is 200 μm, while the channel spacing f_0 is 125 GHz. The spatial dispersion resulting from the diffraction grating is explicitly expressed. The term pf/ f_0 determines the center location of the Gaussian mode, which is a function of the frequency shift f. The output fiber collimator is located laterally off the optical axis of the system, resulting in a phase distribution in the projected field eoutput and therefore the term $\exp\left[jkx \sin\theta_x + jky \sin\theta_y \right]$. Given the exact location

of the output port, θ_x and θ_y can be calculated by either ray tracing or the shift theorem of Fourier transform.

The field distribution einput', the modulated field by the MEMS mirror array, is given by [15]

$$e_{input}(x,y,f)=\left(\frac{2}{\pi\omega_{0x}\omega_{0y}}\right)^{1/2}\exp\left[-\frac{\left(x-\frac{pf}{f_0}\right)^2}{\omega_{0x}{}^2}-\frac{y^2}{\omega_{0y}{}^2}\right]\times\sum_{\zeta=0}^{N-1}A_\zeta\exp[jk[x-\zeta p]\sin\theta_{x\zeta} + jky\sin\theta_{y\zeta}+\phi_\zeta]\mathrm{rect}\left[\frac{x-\zeta p}{p-gap}\right] \quad . \qquad (2)$$

N represents the total number of MEMS mirrors while $\theta_{x\zeta}$ and $\theta_{y\zeta}$ are twice the tilt angles of the ζ^{th} mirror in the x and y directions, respectively. The amplitude attenuation coefficient A_ζ is set to be 1, assuming a perfect mirror surface with 100% reflection. The constant phase $\phi\zeta$ accounts for the mirror sagging. It is set to be 0 in the simulation, assuming a sag-free mirror array.

In our simulation, the mirror of ζ=1 in the array is tilted such that the corresponding wavelength channel is switched to the targeted output fiber collimator. The values of θx1 and θy1 are then determined by the output port coordinate, which varies while rotating the fiber collimator array. For other mirrors without tilt, both $\theta_{x\zeta}$ and $\theta_{y\zeta}$ are 0, implying that the corresponding channels are coupled back to the input port.

The rectangular function results from the finite extent of each mirror. The gap between mirrors has also been taken into account. In our simulation and experiment, mirrors with an octagonal shape are also of interest. It is not as straightforward to have an explicit expression for the octagonal shape embedded in Eq. (2). However, its effect on the coupling efficiency can be addressed by manipulating the integration interval of $\eta=\left|\iint e_{input}'\cdot e^*_{output}dxdy\right|^2$, in which the interval of integration is defined by the mirror areas.

In Eq. (2) the effect of mirror curvature has not been included. If the mirror curvature is to be considered, an additional phase term of $\exp\left[jk\frac{(x-\zeta p)^2+y^2}{R}\right]$ should be incorporated for each mirror, where R is the radius of curvature of the mirror.

III. Simulation Results

For a selected output which is aligned with the input along the horizontal direction (i.e. dispersion direction), the projected image of the output collimator possesses a phase variation along the MEMS mirror array. The gap, which is equivalent to a dark zone between mirrors, leads to a phase jump for any inter-channel wavelength whose field distribution crosses two adjacent mirror pixels. While calculating the coupling efficiency, this results in a non-vanishing overlap integral even if the mirrors are not tilted. On the other hand, if the output is aligned with the input along the vertical direction (i.e. direction orthogonal to dispersion), the projected image of the output then experiences a phase variation along the direction perpendicular to the MEMS mirror array. In this case, the gap introduces no phase jump for the inter-channel wavelengths and hence no inter-channel response is observed. The above comparison is shown in Figure 3. The simulated output spectra [Figure 3(c)] are obtained with perfectly-flat rectangular mirrors. The mirror of ζ=1 is tilted to switch the corresponding channel, f = 125 GHz. For simplicity, the

anamorphic effect arising from the grating has been neglected and the radii of the projected image on the MEMS device plane are set to be $\omega_{0x}=\omega_{0y}=38\mu m$, different than those used for the experiment and the following simulation (ω_{0x} = 69 μm, ω_{0y} = 76 μm).

In our experiment, MEMS mirrors with curvature and an octagonal shape are used. Therefore, the following simulation calculates the power-coupling efficiency vs. frequency shift using such mirror conditions. We consider two different mirror curvatures, R = 30 mm and R = 10 mm. For each curvature, the output spectra under three rotation angles of the collimator array, 0°, 10°, and 20°, are simulated. With 0° rotation, the selected output is aligned with input along the horizontal direction. Figure 4(a) demonstrates the simulation results for R = 30 mm. The arrows indicate the channel centers. When there is no rotation of the collimator array (0°), a pronounced inter-channel response at -27.4 dB below the signal (f = 125 GHz) is exhibited. The inter-channel response is reduced to -31.3 dB (3.9-dB suppression) and -46.3 dB (18.9-dB suppression) below the signal for 10° and 20° rotations, respectively. The results for R = 10 mm are shown in Figure 4(b). When the collimator array is not rotated (0°), an inter-channel response at -23 dB below the signal is observed. Compared with the case of R = 30 mm, the signal level is decreased to -3.1 dB due to a larger mirror curvature. The inter-channel response is suppressed to -26.0 dB (3-dB suppression) and -33 dB (10-dB suppression) below the signal for 10° and 20° rotations, respectively.

It can be seen that the mirror flatness plays an important role and the larger curvature of R = 10 mm has reduced the inter-channel-response suppression, especially for 20° rotation. Greater curvature also increases the dispersion within the passband. For a perfectly-flat (R = ∞) rectangular mirror, the inter-channel response is calculated to be -26.9 dB, -35.1 dB (8.2-dB suppression), and -59.4 dB (32.5-dB suppression) below the signal for rotations of 0°, 10°, and 20°, respectively.

Most wavelength-selective switches have the ability to attenuate signals. In the free-space micromirror-based module, it is done by tuning the mirror angles. For simplicity, we simulate the attenuation functionality using the same parameters as those of Figure 3. It is found that the inter-channel response varies with the attenuation level. For 0° rotation of the 2D collimator array, the inter-channel response between two pass channels with 20-dB attenuation is 5 dB above the attenuated passband signal. When the passband attenuation is increased to 40 dB, the inter-channel response becomes 28 dB above.

IV. Experimental Results

A 1x10 two-axis micromirror array with 200-μm pitch and 98% fill factor is used in the experiment [5], as shown in the inset of Figure 1. The mirrors have radii of curvature within the range of 10±2 mm. The mechanical scan angles are ±2.63° (at 14.1V) and ±1.27° (at 21.1V) for rotation about y and x axes, respectively. The MEMS devices are fabricated using the SUMMiT-V surface micromachining process provided by Sandia National Laboratory. In this prototype system, a 600-grooves/mm grating is used. The focal length of the resolution lens is 30 cm. The channel spacing is 125 GHz. It can be adjusted to comply with the telecommunication-required 50-GHz or 100-GHz spacing by using an 1100-grooves/mm grating, which provides greater dispersion strength and is more commonly used in free-space WDM

systems. A commercial 6x6 collimator array with a 1-mm pitch and a 125-μm beam radius (ω_0) is employed in our system. A 16x telescope expands the optical beams. The collimator array is rotated by small angles (10°, 20°) to mitigate the inter-channel response. Figure 5 shows the spectra from the selected output port at three different rotation angles (0°, 10°, and 20°). The measurement resolution is limited by the optical spectral analyzer available in our laboratory, whose finest resolution bandwidth is 0.08 nm. At 0°, the input and output ports are aligned in the dispersion direction. The dotted lines in Figure 5(a) indicate the positions of channel centers for this WSS. The 1550-nm wavelength is switched to this output port. Signals at other wavelength channels are below ~ -35 dB. However, the response between channels (between dotted lines) are very pronounced (-12.3 dB below the signal). The inter-channel response is reduced to -18.5 dB (6.2-dB suppression) and -20.5 dB (8.2-dB suppression) below the signal at 10° and 20°, respectively. The power level of the OFF channels is higher than those obtained in the simulation as it is eventually clamped by the noise floor of the experiment. The relatively high insertion loss and the suppression deviation from simulation may be due to optical system misalignment, excess mirror curvature, or mirror sagging.

V. CONCLUSIONS AND SELF-EVALUATION (結論及計畫成果自評)

The inter-channel response of a 1xN^2 wavelength-selective switch (WSS) with a two-axis micromirror array has been successfully studied theoretically and experimentally. The simulation results show that the inter-channel response depends strongly on the output port location as well as the MEMS mirror curvature. With 20° rotation of the 2D collimator array, 10-dB and 8.2-dB suppressions are demonstrated theoretically and experimentally, respectively, for a prototype system. Greater suppression of up to 32.5 dB at 20° rotation is expected with perfectly-flat rectangular micromirrors. The Fourier-optics-based model can also be used to calculate the far-field optical pattern in a free-space optical communication system.

Collaboration between UC Berkeley and us (National Taiwan University) was involved in the efforts towards completing this project. Accomplishments related to this project were published in the following journals and conferences:

- ✓ J. C. Tsai et al., "Analysis of the interchannel response in a MEMS 1xN^2 wavelength-selective switch," *OSA Applied Optics*, Vol. 46, No. 16, pp. 3227-3232, June 1, 2007. (SCI, EI)
- ✓ J. C. Tsai et al., "Design, fabrication, and characterization of a high fill-factor, large scan-angle, two-axis scanner array driven by a leverage mechanism," *IEEE/ASME Journal of Microelectromechanical Systems*, Vol. 15, No. 5, pp. 1209-1213, October 2006. (SCI, EI)
- ✓ Z. H. Yu et al., "Simultaneous iterative reconstruction technique for diffuse optical tomography imaging: iteration criterion and image recognition," in *Proc. of SPIE Vol. 6864* (Biomedical Applications of Light Scattering II, BiOS 2008 - part of Photonics West 2008, San Jose, CA, USA, Jan. 2008.), Paper 6864-41. (EI)
- ✓ Z. H. Yu et al., "Diagnosis of cardiovascular diseases based on diffuse optical tomography system," in *Proc. of SPIE Vol. 6864* (Biomedical Applications of Light Scattering II, BiOS 2008 - part of Photonics West 2008, San Jose, CA, USA, Jan. 2008.), Paper 6864-42. (EI)

REFERENCES (參考文獻)

[1] T. Ducellier, J. Bismuth, S. F. Roux, A. Gillet, C. Merchant, M. Miller, M. Mala, Y. Ma, L. Tay, J. Sibille, M. Alavanja, A. Deren, M. Cugalj, D. Ivancevic, V. Dhuler, E. Hill, A. Cowen, B. Shen, and R. Wood, "The MWS 1x4: a high performance wavelength switching building block," ECOC (European Conference on Optical Communication) 2002, Paper 2.3.1.

[2] J. C. Tsai, S. Huang, D. Hah, H. Toshiyoshi, and M. C. Wu, "Open-loop operation of MEMS-based 1xN wavelength-selective switch with long-term stability and repeatability," IEEE Photonics Technology Letters, Vol. 16, No. 4, pp.1041-1043, April 2004.

[3] D. M. Marom, D. T. Neilson, D. S. Greywall, C. S. Pai, N. R. Basavanhally, V. A. Aksyuk, D. O. López, F. Pardo, M. E. Simon, Y. Low, P. Kolodner, and C. A. Bolle, "Wavelength-selective 1xK switches using free-space optics and MEMS micromirrors: theory, design, and implementation," IEEE/OSA Journal of Lightwave Technology, Vol. 23, No. 4, pp.1620-1630, April 2005.

[4] J. C. Tsai, S. Huang, D. Hah, and M. C. Wu, "1xN^2 wavelength-selective switch with two cross-scanning one-axis analog micromirror arrays in a 4-f optical system," IEEE/OSA Journal of Lightwave Technology, Vol. 24, No. 2, pp. 897-903, Feb. 2006.

[5] J. C. Tsai and M. C. Wu, "1×N^2 wavelength-selective switches with tilted 2D collimator arrays for inter-channel-response suppression," in Proceedings of CLEO (Conference on Lasers and Electro-Optics) 2004, paper CTuFF7.

[6] J. C. Tsai and M. C. Wu, "Gimbal-less MEMS two-axis optical scanner array with high fill-factor," IEEE/ASME Journal of Microelectromechanical Systems, Vol. 14, No. 6, pp.1323-1328, December 2005.

[7] J. C. Tsai and M. C. Wu, "Design, fabrication, and characterization of a high fill-factor, large scan-angle, two-axis scanner array driven by a leverage mechanism," IEEE/ASME Journal of Microelectromechanical Systems, Vol. 15, No. 5, pp. 1209-1213, October 2006.

[8] J. C. Tsai and M. C. Wu, "A high port-count wavelength-selective switch using a large scan-angle, high fill-factor, two-axis MEMS scanner array," IEEE Photonics Technology Letters, Vol. 18, No. 13, pp. 1439-1441, July 1, 2006.

[9] D. M. Marom, C. R. Doerr, N. R. Basavanhally, M. Cappuzzo, L. Gomez, E. Chen, A. Wong-Foy, and E. Laskowski, "Wavelength-selective 1x2 switch utilizing a planar lightwave circuit stack and a MEMS micromirror array," in Proceedings of 2004 IEEE/LEOS International Conference on Optical MEMS and Their Applications, pp.28-29.

[10] T. Ducellier, A. Hnatiw, M. Mala, S. Shaw, A. Mank, D. Touahri, D. McMullin, T. Zami, B. Lavigne, P. Peloso, and O. Leclerc, "Novel high performance hybrid waveguide-MEMS 1x9 wavelength selective switch in a 32-cascade loop experiment," Proc. of ECOC (European Conference on Optical Communication) 2004, Paper Th4.2.2

[11] http://www.lightreading.com/document.asp?doc_id=69809&site=ofc

[12] http://www.coadna.com/CoAdna_1x8_2-28-06.pdf

[13] J. E. Ford, V. A. Aksyuk, D. J. Bishop, and J. A. Walker, "Wavelength add-drop switching using tilting micromirrors," IEEE/OSA Journal of Lightwave Technology, Vol. 17, No. 5, pp.904-11, May 1999.

[14] D. M. Marom and S. H. Oh, “Filter-shape dependence on attenuation mechanism in channelized dynamic spectral equalizers,” in Proceedings of LEOS 2002, pp.416-417

[15] S. H. Oh and D. M. Marom, “Attenuation mechanism effect on filter shape in channelized dynamic spectral equalizers,” Applied Optics, Vol.43, No. 1, pp.127-131, Jan. 2004.

[16] R. E. Wagner and W. J. Tomlinson, “Coupling efficiency of optics in single-mode fiber components,” Applied Optics, Vol. 21, pp. 2671–2688, 1982.

[17] J. W. Goodman, Introduction to Fourier optics, McGraw-Hill, c1996.

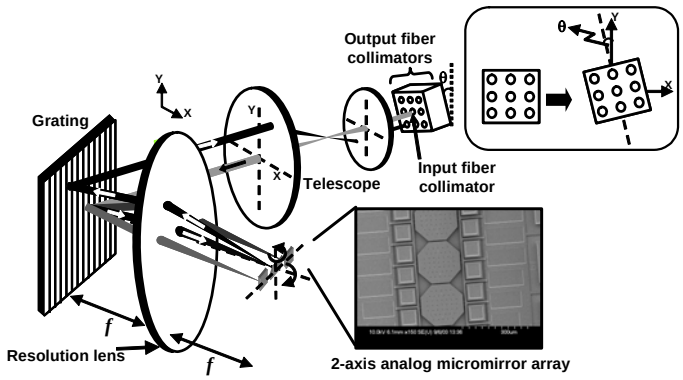

Figure 1 Schematic of the 1xN^2 wavelength-selective switch (WSS) with a rotated 2D collimator array. A two-axis analog micromirror array is used for 2D beam steering. The telescope expands the size of the optical beam.

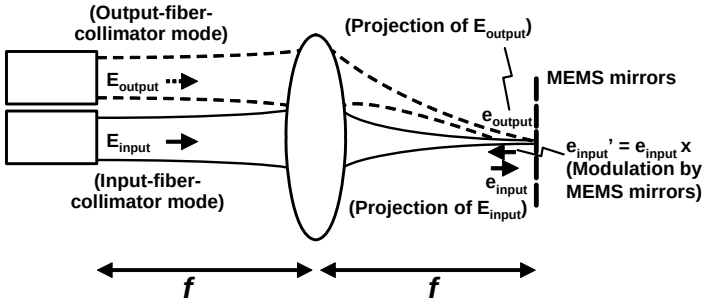

Figure 2 The illustration of the theoretical model based on Fourier optics.

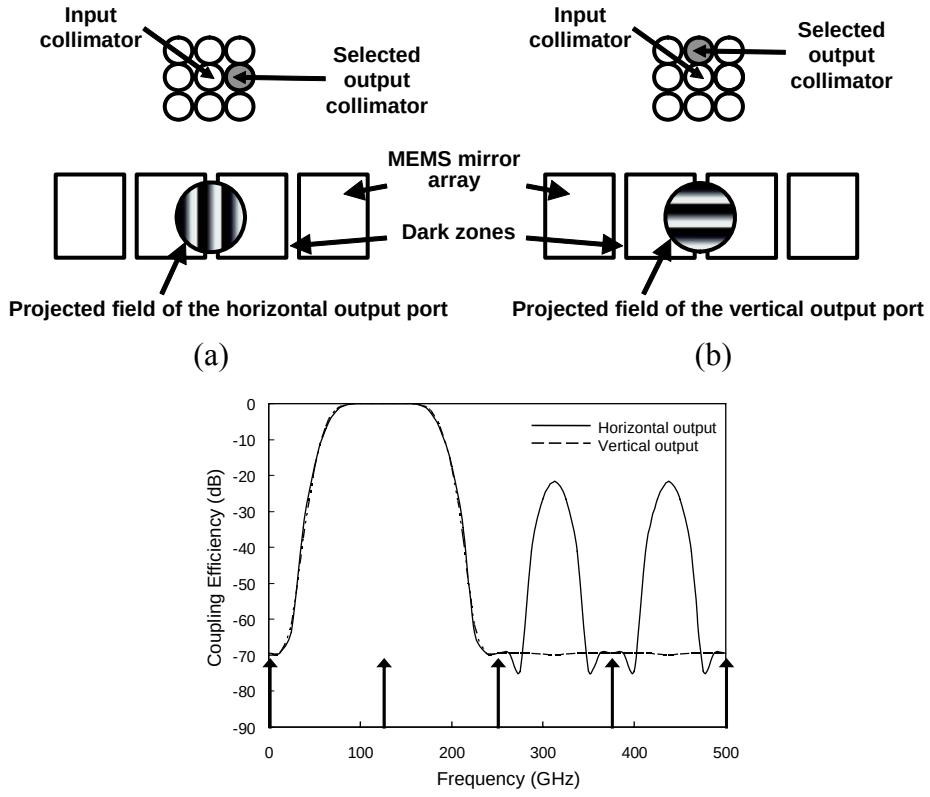

Figure 3 The phase variations of the projected images of (a) a horizontal output port and (b) a vertical output port. The simulation results are shown in (c).

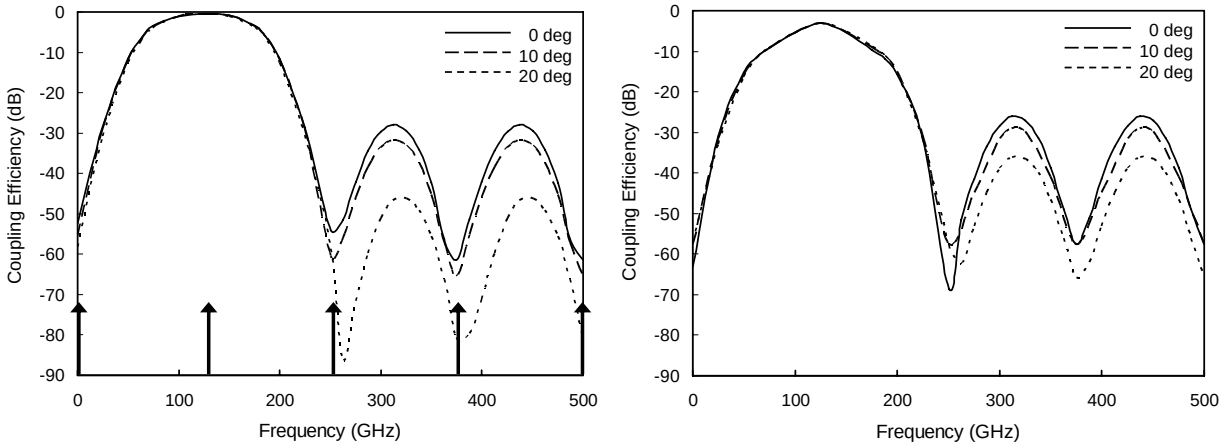

(a) (b)

Figure 4 The simulation results for (a) R = 30 mm and (b) R = 10 mm. Output spectra for each curvature are simulated with 0°, 10°, and 20° rotations of the collimator array. The arrows indicate the channel centers.

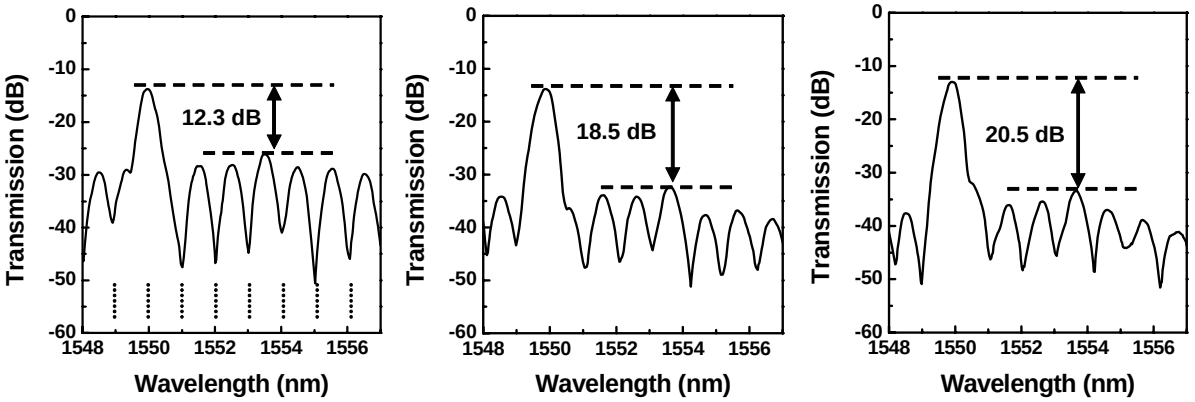

(a) (b) (c)

Figure 5 Optical spectra from a selected output port which is horizontally aligned with the input at 0° rotation, when the collimator array is rotated by (a) 0°, (b)10°, and (c) 20°.The dotted lines in (a) indicate the positions of the wavelength channels. The minor peaks between dotted lines are the inter-channel response.

附件：赴國外出差或研習心得報告

赴國外出差或研習心得報告

計畫編號	NSC 95－2221－E－002－053
計畫名稱	以微機電技術建構之自由空間光通訊系統—用於無人飛行載具或人造衛星間之訊息傳輸
出國人員姓名 服務機關及職稱	蔡睿哲，台灣大學光電工程學研究所，助理教授
出國時間地點	日本神戶，96/1/21-96/1/26
國外研究機構	

工作記要：

出差人員：蔡睿哲〔計畫主持人〕
出差地點：日本神戶
出差日期：96/1/21-96/1/26
出差事由：參加國際會議並與日本公司之研發人員交流

此次出差目的有二：〔一〕參加 20th IEEE International Conference on Micro Electro Mechanical Systems (第 20 屆 IEEE 國際微機電系統會議，會議期間 96/1/21-96/1/25)；〔二〕與日本 TOPCON 公司的研發人員交流。

〔一〕第 20 屆 IEEE 國際微機電系統會議(會議期間 96/1/21-96/1/25)

IEEE International Conference on Micro Electro Mechanical Systems 乃微機電研究領域之一年一度盛事，該會議所涵蓋的範圍包括：製程及封裝技術、材料及元件特性量測、生醫及化學微感測系統、機械及物理感測系統、設計及理論分析、微流體元件及系統、微致動器、光學及射頻微機電系統、能源微機電系統(Energy and Power MEMS)、奈米機電系統等。此會議對於文章的篩選十分嚴格—根據了解，Acceptance Rate 平均為 30%。在被接受的文章中，僅排名前三分之一(換句話說，就是所有投稿文章的 Top 10%)會入選至 Oral Presentation Session；餘下的三分之二(即所有投稿文章中排名 10%-30%)則進入 Poster Session。

此次會議中有許多富啟發性的文章，謹以簡報格式節錄兩篇於下。

V. Milanovic et al. (Adriatic Research Institute, USA), “Highly adaptable MEMS-based display with wide projection angle”：此篇文章中，研究人員使用單一微鏡片掃描雷射光源，以建構一投影顯示系統。

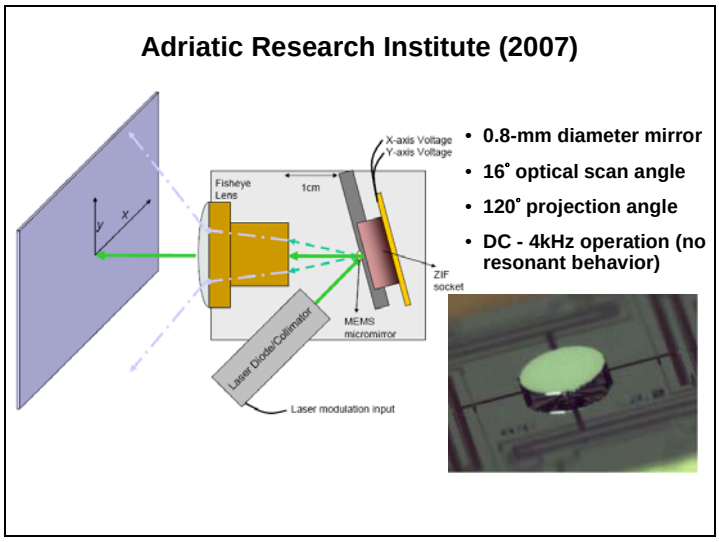

投影光學系統架構及掃描微鏡片之照片

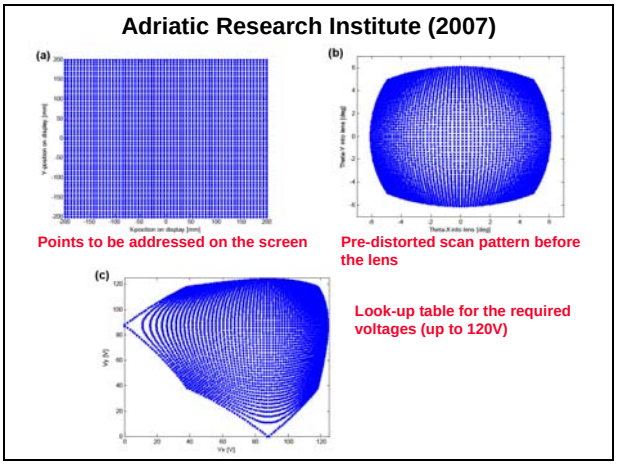

掃描點及驅動電壓之對應圖

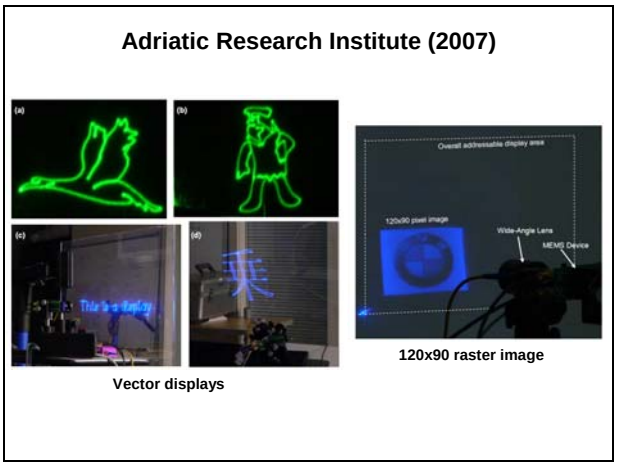

投影影像展示。左方為向量圖，右方為點陣圖。

A. J. Shum et al. (University of Washington), “Vacuum microfabrication on live fruit fly”：此篇文章中，研究人員將活的果蠅置入真空腔體中直接進行沉積(Deposit)製程，果蠅在製程結束後仍可存活。

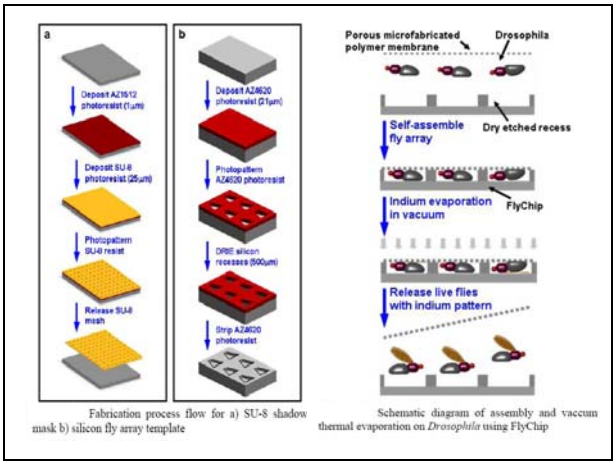

Fabrication process flow for a) SU-8 shadow mask b) silicon fly array template

Schematic diagram of assembly and vaccum thermal evaporation on *Drosophila* using FlyChip

盛裝果蠅之容器〔模子〕的製程及後續於果蠅身上鍍銦〔Indium〕之步驟

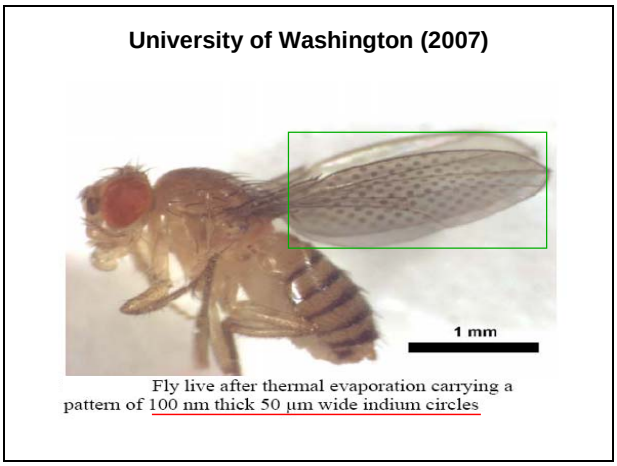

Fly live after thermal evaporation carrying a pattern of 100 nm thick 50 μm wide indium circles

果蠅翅膀上的圓形狀之銦圖樣清晰可見

〔二〕與日本 TOPCON 公司的研發人員交流

此次交流對象為主任研究員(Chief Researcher)藤野誠(Makoto Fujino)與工程師(Opt-Device Engineer)丸山弘毅(Hirotake Maruyama)。藤野主任的研究主要是將微鏡片元件應用於光學測距儀中。